DOI https: //doi. org/10.1007/s11595-023-2703-7

Effects of Coal Metakaolin on the Mechanical Properties and Microstructure of High-belite Sulphoaluminate Cement

WANG Xingyi[1], HAN Pengju[1*], NIU Shiwei[2], HE Bin[1], MA Fuli[1], GUO Tiantian[1], XU Jinchuan[1]

(1. College of Civil Engineering, Taiyuan University of Technology, Taiyuan 030024, China; 2. Yellow River Engineering Consulting Co., Ltd, Zhengzhou 450003, China)

Abstract: The effects of coal metakaolin on the mechanical properties of high-belite sulphoaluminate cement under compressive loading were investigated. The composition and microstructure of hydration products at different hydration times were analyzed by X-ray diffraction and scanning electronic microscopy. The hydration process of blended cement was studied via electrochemical impedance spectroscopy. In particular, replacing a part of cement with CMK (10%, 20%, and 30%) was found to promote the hydration process, to refine the pore size, and to improve the compressive strength of the composite. The best compressive strength of the cement was achieved at a CMK content of 30% after 28 days hydration, being improved by 20.13 MPa, or 1.44 times relative to that of undoped specimens. Furthermore, the compressive strength is shown to correlate with the impedance parameter R_{CCP}, which allows the latter to be used for nondestructive assessment of the compressive strength of blended cement materials.

Key words: coal metakaolin; compressive strength; microstructure; electrochemical impedance spectroscopy; impedance parameter

1 Introduction

With the rapid development of the construction and building industry, cement, especially ordinary portland cement, has become the most popular construction material[1]. However, the cement industry is known for not only its high energy consumption, but also for large CO_2 emissions. In 2019, the global energy-related carbon dioxide emissions have reached 33.1 billion tons. Although CO_2 concentrations have significantly dropped in 2020 due to the impact of COVID-19[2,3], their level still remained high. As the global demand for net zero emissions of greenhouse gases is continuously increasing, the cement industry urgently needs to take active measures to reduce energy consumption and carbon dioxide emissions[4, 5]. To solve this issue, high belite sulphoaluminate cement (HBSC) as a kind of green cement has been proposed[6-8]. Compared with OPC, the preparation of unit mass of HBSC enables one to save 28.57% of limestone and reduce 20.1% of CO_2 emissions[9]. Raupp-Pereira *et al*[10, 11] suggested that the reasons for why CO_2 emissions can be decreased during the preparation of HBSC are as follows. In the mineral design, the dicalcium silicate (C_2S) phase is added to replace the tricalcium silicate (C_3S) phase to reduce the limestone content in the cement composition, thereby further reducing the amount of CO_2 produced during the decomposition of limestone. Also, fast-hardening minerals with low CaO content are introduced for substituting the C_2S phase because of its low hydration rate to ensure the early strength of the cement matrix. Besides, the strength of the β-C_2S phase after two years of hydration is 21% higher than that of the pure C_3S phase. Thus, the later strength of the modified cement exceeds that of traditional portland cement[6,12,13].

Supplementary materials that are widely applied in cement production can reduce production costs and accelerate industrial waste's rational and efficient reuse[14]. Coal metakaolin (CMK) is an amorphous silicon-aluminum compound, which is formed by calcination and dehydration of coal kaolin at an appropriate temperature (600-900 ℃)[15]. Being a type of high-performance mineral admixture, it has recently attracted significant attention in civil engineering[15-17]. CMK is able to exert a direct impact on the composition and micromorphology of the hydration products to improve

(Received: June 14, 2022; Accepted: Sept. 20, 2022)

WANG Xingyi(王星毅): Ph D Candidate; E-mail: wxy19722769115@163.com

*Corresponding author: HAN Pengju(韩鹏举): Prof.; Ph D; E-mail: 13834569544@163.com

Funded by the National Natural Science Foundation of China (No. 41807256)

cement performance. More specifically, owing to the large amount of amorphous active ingredients, such as Al_2O_3 and SiO_2, it has relatively high pozzolanic activity, which can cause gelation under appropriate alkali excitation conditions[18]. Further, it was shown that, compared with a cement matrix, CMK presents an irregular layered structure with a smaller (0.1 to 5 μm) particle size[16,17]. This allows it to fill the pores between cement hydration products and form an overlapping network structure to reduce pore size[19,20]. Therefore, the addition of CMK can decrease the porosity of cement as well as improve its pore structure and overall performance.

Electrochemical impedance spectroscopy (EIS) can use a small amplitude sinusoidal AC voltage as a disturbance signal at different frequencies (f) to monitor the sinusoidal current response of the sample and to obtain its impedance parameters that prerfectly reflect changes in the microstructure of cement materials[21,22]. In the Nyquist plot, the intersection of the high-frequency region and the real axis enables one to obtain the pore solution resistance R_s in the hardened cement paste, which is related to the porosity and ion concentration of the pore solution. In turn, the diameter R_{ct1} of a semicircle in the high-frequency zone can indirectly reflect the OH^- ion concentration in the pore solution of the cement paste[22].

The purpose of this research is to investigate the influence of CMK on the mechanical properties and microstructure of HBSC. Based on the different CMK contents, various groups of specimens were produced and their compressive strength was explored. X-ray diffraction (XRD) and scanning electron microscopy (SEM) was used to study the chemical compositions and microstructure of CMK-doped HBSC to elucidate the influence of CMK on the mechanical properties of HBSC. Also, the hydration process was characterized via EIS, and the microstructural changes in blended cementitious materials were discussed in terms of impedance parameters. This enabled one to establish the correlation between the electrochemical impedance parameter (R_{CCP}) and the compressive strength as a feasible method for nondestructive assessment of the compressive strength in cements.

2 Experimental

2.1 Materials

HBSC with a strength grade of 42.5 was purchased from the Polar Bear Material Company (Tangshan, China). Its chemical and mineralogical compositions are presented in Tables 1 and 2, respectively, and the corresponding XRD diffraction pattern is shown in Fig.1. CMK, provided by the Ju Feng Kaolin Company in Datong, China, served as the supplementary material. Its specific chemical composition is given in Table 3. The apparent density and the specific surface area of HBSC were 2.71 g/cm^3 and 590.1 m^2/kg, respectively. Those of CMK were 2.61 g/cm^3 and 1 792.8 m^2/kg, respectively. Regular tap water without admixtures was used in the experiment, as well. The alkaline stimulator used in the test ($Ca(OH)_2$) was produced by Tianjin Fuchen Chemical Reagent Factory ($Ca(OH)_2 \geqslant 5\%$).

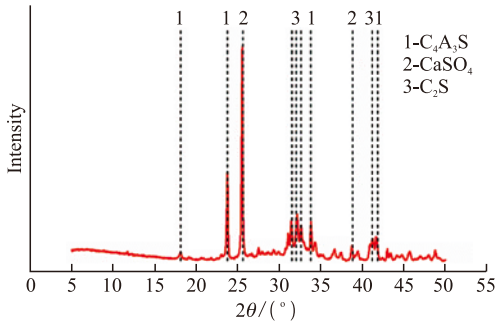

Fig.1 XRD patterns of HBSC

Table 1 Chemical compositions of HBSC

Chemical composition	CaO	SiO_2	Al_2O_3	Fe_2O_3	MgO	SO_3	TiO_2	Sum	Loss
Mass/%	51.54	13.80	15.34	1.52	2.08	14.21	0.71	99.20	0.38

Table 2 Mineralogical compositions of HBSC

Mineralogical composition	$C_4A_3\bar{S}$	C_2S	f-$CaSO_4$	C_4AF	f-CaO	CT
Mass/%	29.35	38.06	13.64	5.08	1.84	1.11

Table 3 Chemical compositions of CMK

Chemical composition	SiO_2	Al_2O_3	Fe_2O_3	TiO_2	CaO	MgO	K_2O	Na_2O	Loss
Mass/%	51.0	44.66	0.96	1.89	0.37	0.24	0.28	0.55	0.05

The content of alkaline activator (calcium hydroxide) was 2% of the total mass of coal metakaolin.

2.2 Materials preparation and characterization

The samples were prepared with CMK contents of 0%, 10%, 20%, and 30% and the constant water-cement ratio of 0.6. The materials for the EIS experiments were cast into 70.7 mm × 70.7 mm× 70.7 mm molds, while those for the compressive strength tests were prepared in molds with dimensions of φ50 mm×100 mm. All the specimens were stored in a curing chamber (95 ± 5% RH, 20 ± 2 ℃) for a specified time.

The compressive strength tests of the samples with different hydration times (1 day, 7, 14, and 28 days) were implemented using a WDW-100compression-testing instrument according to GBT 17671-1999 standard ("Method of testing cements-determination of strength").

The specimens with a 30% CMK content were crushed after 28 days of hydration. Fragments of approximately 10 mm in size were then soaked in alcohol for three days to terminate hydration. Finally, the fragments were removed and ground finely enough to pass through a 0.075 mm sieve. Their XRD analysis was performed using a LabX XRD-6000 diffractometer (Shimadzu, Japan) equipped with a copper X-ray tube operating at 40 kV and 40 mA. The XRD profiles were recorded within a scanning range of 5°-55° and processed by means of MDI Jade software.

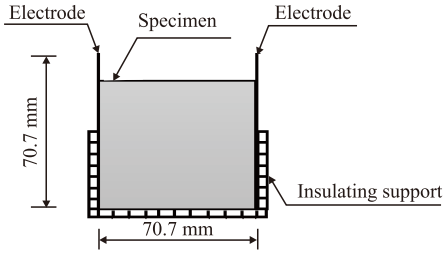

Fig.2 Illustration of the apparatus used for impedance measurements

The microstructure of blended cements was studied using a TM-3000 scanning electron microscope. For this, a test group with a 30% CMK content was selected. The method of termination of hydration treatment of SEM sample is consistent with that of XRD. Prior to the SEM analysis, prismatic samples with dimensions of 20 mm × 20 mm × 10mm were prepared and placed in an oven for heating at 40 ℃ for 12 h. In order to ensure electrical conductivity and avoid the accumulation of the electric charge at the sample surface, vacuum gold plating was performed on the surface of the test block. The vacuum degree for gold plating was 5-6 Pa and the plasma current was less than 10 mA.

A Wuhan Kesite CS350 electrochemical workstation was used to measure the electrochemical impedance of cementitious materials at different hydration times (1 day, 7, 14, and 28 days). During the experiment, the temperature and humidity were respectively kept at 20 ± 5 ℃ and 45% ± 5% RH; Copper electrodes with the same size as the cross-sectional area of the specimen were placed at both ends of the specimen. Then, the specimen was fixed to the electrodes with an insulating fixture, and a certain pressure was applied to ensure that there was a close contact between the sample and the electrodes. The schematic diagram of the device is shown in Fig.2. The AC amplitude was 10 mV, and the frequency range was 10^{-2}-10^{5} Hz. After the testing, the specimens were returned into a standard curing room to continue maintenance. In order to improve the measurement accuracy, the automatic offset was adopted to eliminate the potential and current.

3 Results and discussion

3.1 Compressive strength of blended cements

Fig.3 displays the relationship between the compressive strength and the hydration time of the specimens with different CMK contents. According to the plots, the higher was the hydration time the larger was the compressive strength. With the incorporation of CMK, the growth rate of the early strength of the blended cements was significantly accelerated and the compressive strength of each age increased significantly.

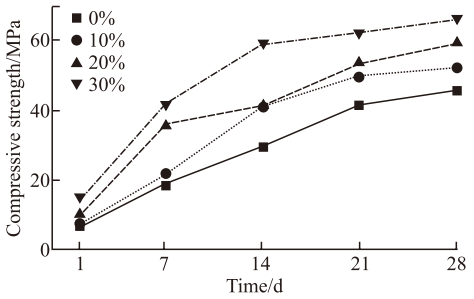

Fig.3 Compressive strengthes of HBSC at different CMK contents and hydration time

In particular, even after 7 days, the compressive strength of the blended cements was in the range of 21.51-41.78 MPa, while that of the specimen without CMK was 18.49 MPa, meaning that the effect of CMK on the early compressive strength of HBSC was remarkable. After 28 days, the compressive strength of CMK-reinforced samples was approximately 50-65 MPa. As seen from the plots, the compressive strength of all the specimens varied noticeably within a period

from 1 day to 21 days, while exhibiting the less pronounced changes in the time range of 21 to 28 days. These data were consistent with the results reported on CMK modified cement soil by Wang *et al*[16] who conducted an unconfined compressive strength test (UCS) and observed no notable increase after 28 days compared to the increment from 7 to 28 days.

The contribution of the pozzolanic effect to the strength of the samples was assessed with respect to the specific strength method proposed by Pu[23]:

$$D = C/A \times 100\%$$

$$C = A - B$$

where, A is the specific strength of HBSC in blended cements, B the specific strength of pure HBSC, and C the specific strength of the pozzolanic effect.

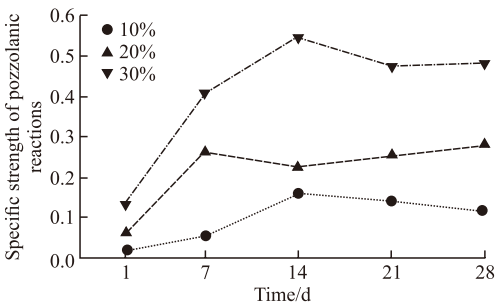

Fig.4 The specific strengthes of pozzolanic effect at different CMK contents and hydration time

Fig.4 displays the relationship between the specific strength of the pozzolanic effect and the hydration time of the specimens with different CMK contents. With the increase of CMK content, the specific strength of the pozzolanic effect at each age increased significantly. With the increase of hydration time, the specific strength of the pozzolanic effect at different CMK contents exhibited first a rapid increase, followed by a slight decrease. Meanwhile, there were differences in the growth rate changes. At the CMK content of 10%, the growth rate of specific strength after 1 day-7 days was lower than that within 7-14 days. In case of the CMK content of 20%, the specific strength increased rapidly in 1 day-7 days and then decreased gently after reaching its peak value after 7-14 days. At the CMK concentration of 30%, the growth rate of specific strength after 1 day-7 days was greater than that within 7-14 days. After 28 days of hydration, blended cement with a 30% CMK content was 4 times that of the cement with a 10% CMK concentration.

Therefore, the incorporation of CMK could promote the formation of cement strength, especially for early strength. The promotion effect on cement hydration was less pronounced at 10% CMK content, and the incidence of pozzolanic reactions was also lower. This could explain why the growth rate of 10% CMK content was lower in 1 day-7 days. In turn, using 20% and 30% CMK content resulted in the larger contact area with a cement clinker, which might have obviously promoted cement hydration, and the pozzolanic reactions might have occurred earlier. This was also conducive to the rapid increase in the strength of cements with 20% and 30% CMK contents within 1 day-7 days. Moreover, a decrease in the specific strength of the cements after reaching the peak value was observed independently of the amount of CMK used. This indicated that the incorporation of CMK might have induced some reactions after 14 days, thereby inhibiting the further progress of the pozzolanic reaction.

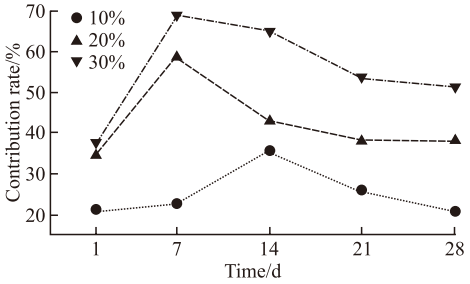

Fig.5 The contribution rate of pozzolanic effect at different CMK contents and hydration time

Fig.5 displays the relationship between the contribution rate of pozzolanic effect to compressive strength and the hydration time of the specimens with different CMK contents. Increasing the content of CMK, the contribution rate of pozzolanic reactions to compressive strength increases significantly. For the 10% CMK content, the extreme point of the intensity contribution rate appeared at 14 days, and decreased after 14 days, and there was a 20% strength contribution rate at 28 days. When the CMK content is 30%, the contribution rate of the pozzolanic reactions to the compressive strength rised rapidly at 1 day-7 days, and reaches 70% at 7 days, and then decreases. However, after 21 days, the contribution rate of the pozzolanic reactions to the compressive strength remained within a relatively stable range. At 28 days, it can still reach a strength contribution rate of more than 50%. This shows that CMK has an obvious promotion effect on the formation of early strength of cement, and has a great contribution to the improvement of later strength. The mixing amount of CMK will significantly affect the formation of early strength of cement. When the mixing amount is small, the pozzolanic reaction will have a certain hysteresis.

A significant impact of CMK on the compressive strength of HBSC was mainly due to the combination of the filling and acceleration effects along with the pozzolanic reactivity. The impact was especially pronounced after 1 day-14 days, which was similar to that reported by Wild *et al*[24] who observed metakaolin causing the immediate filling effect, the noticeable acceleration of the ordinary portland cement within the first 24 h and the influence of the pozzolanic reaction between 7 and 14 days.

3.2 XRD analysis of hydration products

In cement scientific research, XRD is used to qualitatively analyze the composition of hydration products at different hydration times[25]. The main products of high-belite sulfoaluminate cement may include ettringite (AFt), monosulfide hydrated calcium sulfoaluminate (AFm), aluminum hydroxide (AH_3), and hydrated calcium silicate (C-S-H) phases.

The XRD pattern of high-belite sulphoaluminate cement with a 30% CMK content after 28 days of hydration is shown in Fig.6. Here, the main diffraction peaks correspond to the hydration products such as AFt, AFm, AH_3, and C-S-H gel. And there are also the reflexes associated with partially unhydrated C_2S.

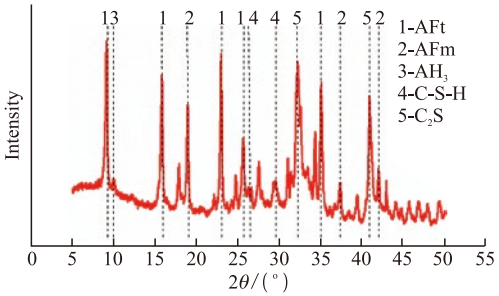

Fig.6 XRD patterns of blended cement after 28 days of hydration

After 28 days of hydration, the characteristic peaks of $C_4A_3\bar{S}$ and $CaSO_4$ phases disappeared completely, but those of AFt dramatically increased. This indicates that the hydration reaction between $C_4A_3\bar{S}$ and $CaSO_4$, completely consuming both reactants, could have generated a large amount of AFt phase [26]:

$$C_4A_3\bar{S}+2C\bar{S}+38H \rightarrow C_3A\cdot 3C\bar{S}\cdot 32H+2AH_3 \quad (1)$$

Besides, the characteristic peaks of the AFm phase could be observed. This is because, under the condition of insufficient $CaSO_4$ content, $C_4A_3\bar{S}$ hydrated to form the AFm phase(Eq.2) [26], and there was a conversion from AFt to the AFm phase (Eq. 3).

$$C_4A_3\bar{S}+2C\bar{S}+18H \rightarrow C_3A\cdot 3C\bar{S}\cdot 12H+2AH_3 \quad (2)$$

$$C_3A\cdot 3C\bar{S}\cdot 32H \rightarrow C_3A\cdot 3C\bar{S}\cdot 12H+2CSH_2+16H \quad (3)$$

Furthermore, the characteristic peaks of C_2S were also very strong, which indicated that most of C_2S had not undergone the hydration yet. This was owing to the fact that the hydration rate of C_2S was lower than that of $C_4A_3\bar{S}$, and the corresponding reaction was as follows[27, 28]:

$$C_2S+2H \rightarrow C\text{-}S\text{-}H+CH \quad (4)$$

Therefore, a broadened peak of the C-S-H phase could be observed in the XRD pattern of the hydrated product. This was associated with a certain amount of gelatinous C-S-H produced through the hydration of C_2S (Eq.(4))[19]. However, there were no peaks of CH in the XRD pattern of the hydrated product, and the signature assigned to AH_3 gel was also very weak. This could be explained by the fact that CH and AH_3 gels were produced during the hydration process[29]. However, there was a chemical reaction to form ettringite, wherein the hydration products AH_3 and CH underwent secondary hydration due to the presence of $CaSO_4$[27,28,30]:

$$AH_3+3CH+3C\bar{S}+26H \rightarrow C_3A\cdot 3C\bar{S}\cdot 32H \quad (5)$$

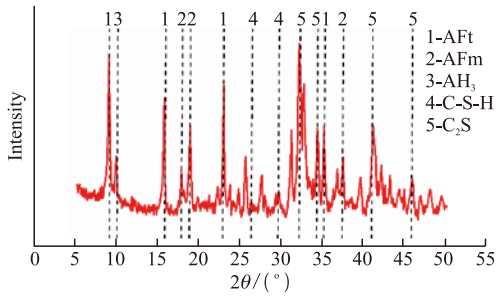

Fig.7 XRD patterns of HBSC after 28 days of hydration

Since many forms of calcium aluminate hydrate are produced in the course of hydration, their characteristic peaks overlap in the XRD pattern, making it difficult to distinguish between single phases. Besides, the instable structure of calcium aluminate hydrate is prone to crystal form conversion during the drying of the specimens, which has a certain impact on the analysis of hydrated products. Therefore, only AFm represents a complex form of multiple calcium aluminate hydrates. In detail, the hydration system of HBSC is Al_2O_3-CaO-SiO_2-H_2O and the hydration reaction involves more intermediate products and secondary reactions. There are many possible kinds of phases in this system, such as C_4AH_{19}, C_4AH_{13}, C_3AH_6, C_2ASH_8, and CAH_{10}[30].

Comparing these data with the XRD pattern of HBSC at the same hydration time (Fig.7)[30], noticeable differences in the hydration process of both materials could be concluded. In the part of HBSC specimens with a 30% CMK content, the characteristic peak of C_2S was relatively lower. In turn, the reflex of C-S-H gel was significantly higher, whereas those of CH and AH_3 gel were almost hard to find in the XRD patterns during the hydration process. This mismatch was owing to various reasons. First, due to the incorporation of CMK, there were more Al^{3+} ions in the pore solution in the early stage of hydration and the nucleation process of the C-S-H gel was inhibited, so that the C_2S phase reaction rate was lower. With the increase of pH of the system and Ca^{2+} ion concentration, the hindering effect of Al^{3+} ions in the nucleation of C-S-H gel weakened significantly, thereby accelerating the hydration of C_2S and generating a large amount of C-S-H gel (Eq.(4)). Second, CMK will also participate in the hydration reaction, consuming a large amount of CH and producing the additional C-S-H gel and AFm. The pozzolanic reactions between CMK and CH can be described by the equations below [30]:

$$AS_2+3CH+6H \rightarrow C_2ASH_8+C\text{-}S\text{-}H \quad (6)$$

$$AS_2+5CH+3H \rightarrow C_3AH_6+2C\text{-}S\text{-}H \quad (7)$$

$$AS_2+6CH+9H \rightarrow C_4AH_{13}+2C\text{-}S\text{-}H \quad (8)$$

where, AS_2 ($Al_2O_3{\cdot}2SiO_2$) is the major reactive substance of CMK. It can be responsible for the increase in compressive strength of the test group by 43.9%, caused by the addition of the 30% CMK content. Therefore, the incorporation of CMK would largely improve the properties of blended cement because more hydration products would be produced due to the pozzolanic reactivity and accelerating effects of the CMK.

3.3 SEM analysis of hydration products

The performance of cement materials not only depends on the composition of related hydration products, but to a large extent on their microstructure. The SEM images of blended cements (30% CMK) after different hydration times (1 day, 7, 14, and 28 days) are shown in Fig.5.

As seen in Fig.8(a), after one day of hydration, plenty of needle-like AFt phases and small size hexagonal flakes of the AFm phase were formed. Also, numerous hydration cement clinker particles could be observed. According to Fig.8(b), after 7 days of hydration, with the incorporation of CMK, the hydration reaction of HBSC was accelerated and CMK participated in the hydration reactions respect to Eqs.(6)-(8). The layered AFm phase and spherical C-S-H gel particles obviously increased. The latter ones, in turn, filled the pores of the AFt-AFm network structure, making the material structure denser. Meanwhile, it was difficult to find the CH phase in the SEM images, meaning that its content in the hydration product was substantially low, which was consistent with the above XRD results (Fig.7). As seen from Figs.8(c) and 8(d), the long-term hydration caused an increase in the amount of the products and the microstructure densification. After 28 days, the AFt inclusions were transformed into rods and columns, interspersed with AFm, and interlaced to form a stable net-like skeleton. At the same time, with the incorporation of CMK, a large amount of fibers and spheres C-S-H gel was generated. These afterwards filled the pores and enhanced the connection between the structural framework, which was conducive to filling and cementing, but significantly reduced the porosity of the blended cement. As a result, the CMK-modified composite had higher compressive strength.

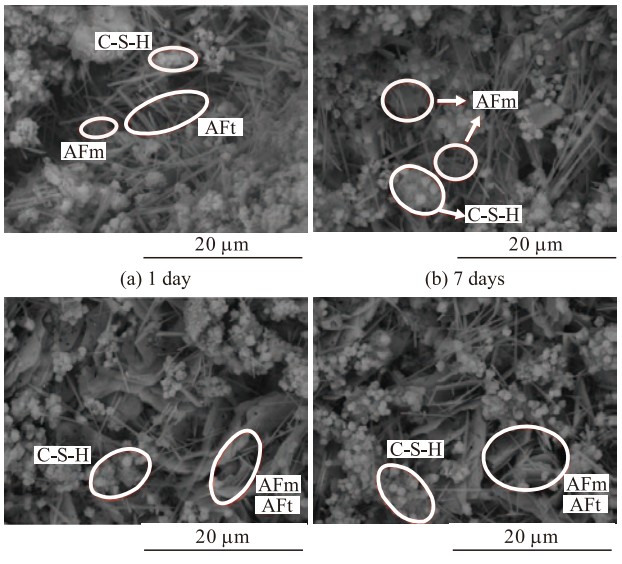

Fig.8 SEM images of blended cement after different hydration time

3.4 Analysis of Nyquist plots

Nyquist plots are often used in the analysis of electrochemical impedance spectroscopy (EIS) data and consider both the real (Z') and imaginary (Z'') parts of the impedance. The impedance results measured at different frequencies are expressed on a complex plane without directly reflecting the magnitude of the frequency. Nyquist diagrams allow one to assess the impedance changes by the equivalent circuit to express the changes in the microstructure during the hydration of the cement.

Four sets of experiments were carried out in this study according to various CMK contents (0%, 10%, 20%, and 30%). The Nyquist plots of the blended cements at different hydration times (1 day, 3, 7, 14, and 28 days) are illustrated in Fig.9.

After one day of hydration (Fig.9(a)), the Nyquist plots were basically straight lines with no pronounced curve characteristics. This indicated the absence of intensive electrochemical reactions in the blended cement, the electrochemical reaction could only have occurred on the rough surface of the C-S-H gel and proceeded once the C-S-H gel has achieved its certain amount[31,32]. Therefore, the hydration degree of C_2S was still low after one day of hydration. Only a small quantity of the C-S-H gel was generated, being far from that sufficient for a significant electrochemical reaction.

After 3 days of hydration (Fig.9(b)), the impedance curves were basically the same, beginning to shift toward the Quasi-Randles curves. In the high-frequency area, the semicircle capacitive loop appeared, indicating a certain amount of C-S-H gel already existed in the blended cement. In addition, with the increase of CMK content, the diameter of the semicircular capacitive loop in the high-frequency region reflecting the resistance of hydrated electrons in the charge transfer process increased significantly. The latter, in turn, was susceptible to changes in the microstructure, being closely related to the average pore size and porosity of the material. Besides, an increase in the diameter of the high-frequency semicircular capacitive loop with rising CMK concentration enhanced the compactness of the blended cement and reduced its porosity [17]. The reasons for the above phenomenon were as follows. On the one hand, CMK has a strong adsorption effect on water molecules because of its smaller particle size, larger specific surface area, and stronger surface activity, which can increase the consistency of cement and hinder the migration of ions in the pore solution. On

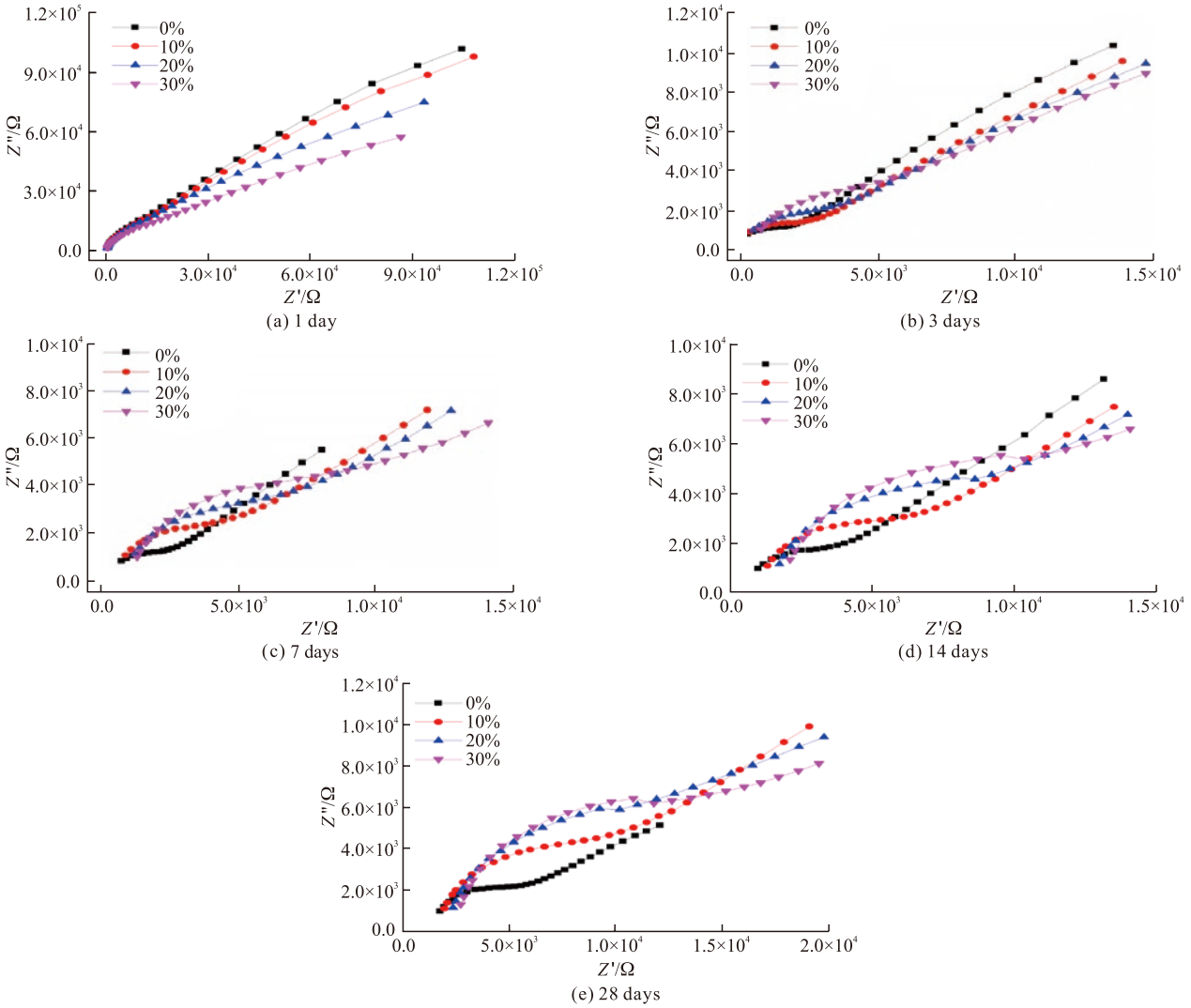

Fig.9 The Nyquist plots for different hydration periods

the other hand, the addition of CMK could accelerate the early hydration rate of HBSC[24, 33].

With the progress of hydration (Fig.9(c)), the effect of CMK became very significant. At the same hydration time, the semicircular capacitive loop diameter of the test groups containing CMK was much greater than that without CMK. Comparing with the data for different test groups after 3, 7, and 14 days, it can be found that, with the increase of hydration time, the semicircular capacitive loop diameter in the high-frequency zone dramatically increased with the increase of CMK content. Also, the straight-line slope in the low-frequency region rapidly decreased with increasing CMK concentration. In general, the electrochemical reaction inside the CMK-containing cement took place earlier than that in the cement without CMK. And with the increase of CMK content at the same hydration time, the semicircular capacitive loop diameter in the high-frequency zone increased, which indicated that the incorporation of CMK significantly accelerated the rate of hydration reaction and hydration process of the blended cement. The decrease in the slope of the oblique straight line in the low-frequency region indicated an increase in the CMK content, making it difficult the ion diffusion. Therefore, compared with the specimen without CMK, the structure of blended cement was denser due to the added CMK. This well explains the rapid increase in compressive strength of blended cements with CMK after 7 days of hydration.

After 14 and 28 days (Figs.9(d) and 9(e)), the diameters of the semicircle capacitive loops in the high-frequency zone of specimens continued to grow. But the growth rate and amplitude were significantly lower as compared to those in Fig.6(c), exhibiting the characteristics of a stable hydration period. This phenomenon was consistent with the slower growth rate of the compressive strength of CMK-reinforced cement from 14 to 28 days.

3.5 Equivalent circuit model

Generally, cement-based materials can be considered the specific electrochemical systems[34]. Due to their internal porous structure and the existence of pore solution, the hydration process induces a significant alteration in their internal structure, which can monitored via EIS[21]. Consequently, the EIS method is applicable for investigating the hydration process of HBSC with CMK. The electrochemical impedance spectrum and the corresponding impedance parameters of the blended cement can be obtained by the electrochemical test method, which allows one to elucidate the hydration mechanism occurring in the material.

To date, numerous equivalent circuit (EC) models have been proposed for the analysis and interpretation of the Nyquist plots and impedance parameters to describe the hydration process in cements[35-37]. However, in some cases, the existing EC approaches fail to simulate the cementitious specimen because of some limitations. For example, the model developed by Gu[38] and expressed as R_s (C_1R_{ct1}) (C_2R_{ct2}) considers the electrode influence of a cementitious material and the external test electrode. However, the dispersion effect, that is, the deflection of the impedance spectrum curve of the composite, is neglected.

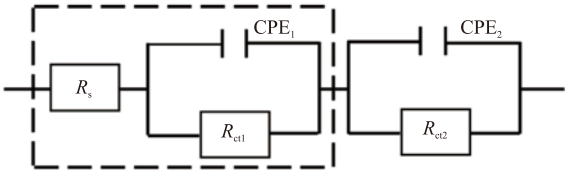

Fig.10 Modified equivalent circuit model

To obtain accurately the electrochemical parameters, we modified the EC model proposed by Gu by replacing the capacitor with a constant phase element (CPE), so that it could be described as R_s(CPE$_1R_{ct1}$) (CPE$_2R_{ct2}$) (see Fig.10). The circuit of a cement matrix is located within the dashed box and the other part is the external test electrode. Since the external test electrode exerts a little influence on the cement hydration process, it is not considered in this study. The role of each parameter in these models is as follows: R_s is the

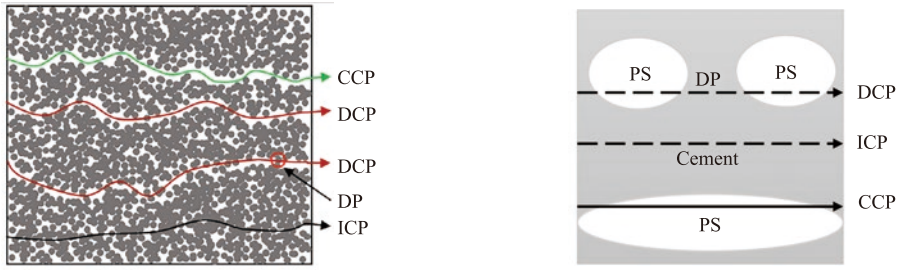

(a) Schematic representation of the microstructure of cement (b) Simplified microstructure of cement

Fig.11 Microstructure of cement materials

electrolyte resistance in the pore solution; CPE_1 the constant phase element that represents the electrical double layer capacitance between the solid and liquid phases; R_{ct1} the resistance of the charge transfer process in the cement specimen.

The cement specimen is composed of a solid part (hydration products and unhydrated cement) and pores, and its microstructure is schematically illustrated in Fig.11(a) [22]. In such a structure, there are three different conductive paths: a continuous conductive path (CCP), a discontinuous conductive path (DCP), and an insulator conductive path (ICP). Correspondingly, the microstructure of cement can be simplified as shown in Fig.11(b), where the grey and white areas represent the solid part and pores, respectively. In addition, PS means the pore solution and DP is the discontinuous point.

Based on the comparative analysis and simplification of multiple EC models in the relevant research[22], the equivalent circuit components and cement microstructure can be connected, and the following relationships can be established:

$$R_{CCP} = R_S + R_{ct1} \tag{9}$$

$$R_{CCP} = (R_S + R_{ct1})R_S/R_{ct1} \tag{10}$$

$$R_{CP}/R_{CCP} = R_S/R_{ct1} \tag{11}$$

$$R_{DP} = CPE_1[R_{ct1}/(R_S + R_{ct1})]^2 \tag{12}$$

The significance of each parameter in the above equations is as follows: R_{CCP} is the total impedance of all the CCPs in the blended cement; R_{CP} the resistance of the connected part of DCPs; C_{DP} the capacitance of the DP point of DCP, which are treated as a double parallel plate capacitance[22].

3.6 Analysis of the impedance parameters

The microstructural characteristics of blended cements govern their mechanical properties. Based on the proposed EC model, the Nyquist plots of the cement materials with different CMK contents and hydration times were fitted to obtain the impedance parameter values (R_s, R_{ct1}, and CPE_1). Thus, the impedance parameters R_{CCP} and R_{CP} can be calculated by formulas (9) to (12), which are sensitive to the ion concentration in the pore solution and the porosity of cement materials. That is, any changes in the microstructure of the material will cause alterations in these parameters, therefore making them important for present research.

The impedance parameter R_{CCP} of the blended cement is shown in Fig.12 as a function of hydration time. The obtained curves were similar to those of compressive strength (Fig.3), exhibiting an increasing trend with the hydration time and reflecting the remarkable effect of incorporated CMK on the value of R_{CCP}. Compared with the undoped specimen, the value of R_{CCP} for the test groups was increased by 1.84-3.95 times after 7 days and by 1.64-2.45 times after 28 days. Moreover, the value of R_{CCP}, which indicated the total impedance of all the CCPs in the blended cement, was inversely proportional to the ion concentration in the pore solution and the porosity of the blended cement[22]. The larger was the parameter value, the stronger was the compactness of the microstructure.

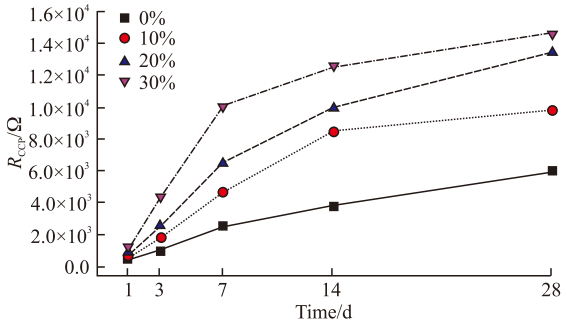

Fig.12 Impedance parameter R_{CCP} as a function of hydration time

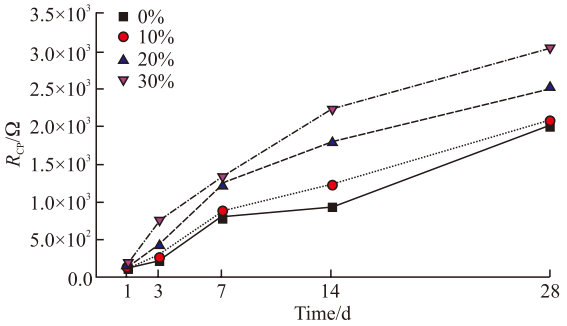

Fig.13 Impedance parameter R_{CP} as a function of hydration time

The impedance parameter R_{CP} of the blended cement at different hydration times is plotted in Fig.13. It can be seen from the figure that the parameter value increased with increasing hydration time. It is noteworthy that the parameter R_{CP} reflects the state of disconnected pores. Furthermore, its behavior was similar to that of R_{CCP}, showing the rapid growth in the early stage and the slower one at the final stage of hydration.

This could be due to the following reasons. First, the incorporation of CMK increases the early hydration rate of blended cement and dramatically accelerates its hydration reaction[39]. In the early stage, the hydration products like needle-like AFt, small-size hexagonal AFm flakes and spherical C-S-H gel particles will fill the conductive paths without blocking the CCPs.

Second, the addition of CMK improves the degree of hydration of the blended cement and its participation in the hydration process[40]. Furthermore, C-S-H gel and AFm were produced by the pozzolanic reactions and adsorbed to a needle-like AFt structure that was afterwards transformed into a rod-shaped one. This will further increase the values of electrochemical parameters (R_{CCP} and R_{CP}). Third, there is a large number of rod-shaped and column-shaped AFt inclusions formed in the later stage, and due to the overlapping and adsorption of AFm and C-S-H gel, a certain dense structure may completely block a part of the point-to-point channel. As a result, some CCPs are blocked by the hydration products and turned into DCPs, which leads to a slowdown in the parameter value growth rate to some extent. Furthermore, while the R_{CCP} value has dropped significantly, the R_{CP} parameter exhibited a slow decrease.

By comparing the two parameters with each other, R_{CCP} is found to be more sensitive to microstructural changes, as concluded from its greater amplitude of variation. In this respect, we further considered it as the main indicator for the investigation of the cement microstructure. Since the microstructure is closely related to the mechanical properties, especially the compressive strength, the next part of the current research will be aimed at establishing the relationship between the impedance parameter R_{CCP} and the compressive strength.

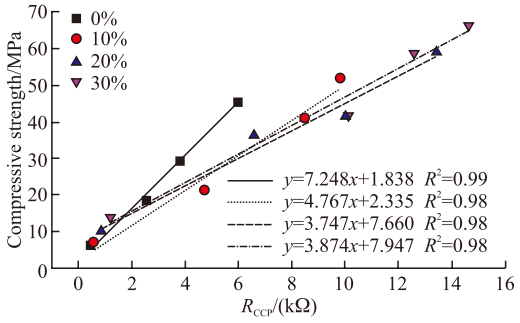

Fig.14 The correlation between the compressive strength and R_{CCP}

Fig.14 displays the correlations between the R_{CCP} values and the compressive strength of the cement materials with different CMK contents. The obtained plots were fitted using the linear function $y = ax + b$. All the goodness-of-fit coefficients, R^2, were greater than 0.94, indicating a strong relationship between the two parameters. The slopes of the fitting curves decreased with increasing CMK content from 0 to 20%, remaining almost unchanged with a further increase in dopant concentration. Therefore, based on the modified equivalent circuit model, it is feasible to predict the compressive strength of cement materials by only determining the parameter R_{CCP} via electrochemical impedance spectroscopy.

4 Conclusions

In this study, the effects of CMK on the properties of high-belite sulphoaluminate cement were investigated. The mechanical properties of CMK-HBSC blended cement were investigated by compressive strength. The hydration process of the blended cements at the microstructural level was studied by means of XRD, SEM and EIS techniques. Based on the results, the main conclusions of present research can be drawn as follows:

a) CMK could accelerate the formation of strength in the cement and had a remarkable enhancement effect on the early and late stages of strength. The higher was the CMK content, the greater was the compressive strength of the cement.

b) The incorporation of CMK did not change the composition of HBSC hydration products but exerted a large impact on the hydration reactions themselves. In particular, according to the XRD results, CMK participated in the hydration process, consuming a large amount of $Ca(OH)_2$ and promoting the increase of hydration products, which had a significant promotion effect on the formation of the AFm and C-S-H gel phase. Compared with cement particles, the hydration products had a denser structure.

c) EIS enabled one to reflect the hydration degree and internal microstructural changes of blended cements. As the hydration time increased, the Nyquist plots shifted toward the typical Quasi-Randles profiles. Each EIS curve of cements was composed of a semicircle capacitive loop with a certain offset at high frequency and an oblique straight line at low frequency. And with the increase of CMK content, the curve continuously moved to the right, whereas the diameter of semicircular capacitive loops increased. Namely, with the incorporation of CMK, the blended cement had a denser internal structure.

d) The impedance parameter R_{CCP} showed the increasing trend similar to that of the compressive strength, with a rapid growth in the early stage and a slow one in the later stage of hydration. The larger was the parameter value, the stronger was the microstructure compactness of blended cement. Furthermore, a linear relationship between the impedance parameter R_{CCP} and the compressive strength was established,

making it possible to nondestructively assess the compressive strength of cementitious materials using the impedance parameter.

References

[1] Nasr MS, Hasan ZA, Abed M K, *et al*. Utilization of High Volume Fraction of Binary Combinations of Supplementary Cementitious Materials in the Production of Reactive Powder Concrete[J]. *Periodica Polytechnica Civil Engineering*, 2020, 65: 335-343

[2] Quéré CL, Jackson RB, Jones MW, *et al*. Temporary Reduction in Daily Global CO_2 Emissions during the COVID-19 Forced Confinement[J]. *Nature Climate Change*, 2020, 10: 647-653

[3] Forster PM, Forster HI, Evans MJ, *et al*. Current and Future Global Climate Impacts Resulting From COVID-19[J]. *Nature Climate Change*, 2020, 10: 913-919

[4] Shubbar AA, Jafer H, Abdulredha M, *et al*. Properties of Cement Mortar Incorporated High Volume Fraction of GGBFS and CKD from 1 day to 550 Days[J]. *Journal of Building Engineering*, 2020, 30: 101 327

[5] Nasr MS, Shubbar AA, Abed ZAR, *et al*. Properties of Eco-friendly Cement Mortar Contained Recycled Materials from Different Sources[J]. *Journal of Building Engineering*, 2020, 31: 101 444

[6] Liu C, Luo JL, Li QY, *et al*. Calcination of Green High-belite Sulphoaluminate Cement (GHSC) and Performance Optimizations of GHSC-based Foamed Concrete[J]. *Materials & Design*, 2019, 182: 107 986

[7] Zhang WQ, Zhu XX, Xu SX, *et al*. Experimental Study on Properties of a New Type of Grouting Material for the Reinforcement of Fractured Seam Floor[J]. *Journal of Materials Research and Technology*, 2019, 8: 5 271-5 282

[8] Gartner E, Sui TB. Alternative Cement Clinkers[J]. *Cement and Concrete Research*, 2018, 114: 27-39

[9] Li J. *Study on High Belite-sulphoaluminate Cement*[D]. Wuhan: Wuhan University of Technology, 2013 (In chinese)

[10] Iacobescu RI, Pontikes Y, Koumpouri D, *et al*. Synthesis, Characterization and Properties of Calcium Ferroaluminate Belite Cements Produced with Electric Arc Furnace Steel Slag as Raw Material[J]. *Cement and Concrete Composites*, 2013, 44: 1-8

[11] Raupp-Pereira F, Ball RJ, Rocha J, *et al*. New Waste Based Clinkers: Belite and Lime Formulations[J]. *Cement and Concrete Research*, 2008, 38: 511-521

[12] Gong YF, Fang YH. Preparation of Belite Cement from Stockpiled High-carbon Fly Ash using Granule-hydrothermal Synthesis Method[J]. *Construction and Building Materials*, 2016, 111: 175-181

[13] Martín-Sedeño MC, Cuberos AJM, De la Torre ÁG, *et al*. Aluminum-rich Belite Sulfoaluminate Cements: Clinkering and Early Age Hydration[J]. *Cement and Concrete Research*, 2010, 40: 359-369

[14] Cai LX, Li XG, Ma BG, *et al*. Effect of Binding Materials on Carbide Slag Based High Utilization Solid-wastes Autoclaved Aerated Concrete (HUS-AAC): Slurry, Physic-mechanical Property and Hydration Products[J]. *Construction and Building Materials,* 2018, 188: 221-236

[15] Siddique R, Klaus J. Influence of Metakaolin on the Properties of Mortar and Concrete: A Review[J]. *Applied Clay Science*, 2009, 43: 392-400

[16] Wang LH, Li XY, Cheng Y, *et al*. Effects of Coal-bearing Metakaolin on the Compressive Strength and Permeability of Cemented Silty Soil and Mechanisms[J]. *Construction and Building Materials*, 2018, 186: 174-181

[17] Wang LH, Li XY, Cheng Y, *et al*. Effects of Coal-metakaolin on the Properties of Cemented Sandy Soil and Its Mechanisms[J]. *Construction and Building Materials,* 2018, 166: 592-600

[18] Zhang AY. Effect of Epoxy Resin on Mechanical Properties of Metakaolin Based Geopolymer and Microscopic Analysis[J]. *Journal of Wuhan University of Technology-Mater. Sci. Ed.*, 2020, 35: 431-434

[19] Wu ZL, Deng YF, Liu SY, *et al*. Strength and Micro-structure Evolution of Compacted Soils Modified by Admixtures of Cement and Metakaolin[J]. *Applied Clay Science*, 2016, 127-128: 44-51

[20] Zhang TW, Yue XB, Deng YF, *et al*. Mechanical Behaviour and Micro-structure of Cement-stabilised Marine Clay with a Metakaolin Agent[J]. *Construction and Building Materials*, 2014, 73: 51-57

[21] Dong BQ, Li G, Zhang JC, *et al*. Non-destructive Tracing on Hydration Feature of Slag Blended Cement with Electrochemical Method[J]. *Construction and Building Materials*, 2017, 149: 467-473

[22] Song GL. Equivalent Circuit Model for AC Electrochemical Impedance Spectroscopy of Concrete[J]. *Cement and Concrete Research*, 2000, 30: 1 723-1 730

[23] Pu XC. Study on the Pozzolanic Effect of Active Mineral Admixtures in Cement and Concrete by Using Specific Strength Index[J]. *China Concrete and Cement Products*, 1997, 3:6-14 (In chinese)

[24] Wild S, Khatib JM, Jones A. Relative Strength, Pozzolanic Activity and Cement Hydration in Superplasticised Metakaolin Concrete[J]. *Cement and Concrete Research*, 1996, 26: 1 537-1 544

[25] Goergens J, Manninger T, Goetz-Neunhoeffer F. In-situ XRD Study of the Temperature-dependent Early Hydration of Calcium Aluminate Cement in a Mix with Calcite[J]. *Cement and Concrete Research*, 2020, 136: 106160

[26] Winnefeld F, Martin LHJ, Müller CJ, *et al*. Using Gypsum to Control Hydration Kinetics of CSA Cements[J]. *Construction and Building Materials*, 2017, 155: 154-163

[27] Morin V, Termkhajornkit P, Huet B, *et al*. Impact of Quantity of Anhydrite, Water to Binder Ratio, Fineness on Kinetics and Phase Assemblage of Belite-ye'elimite-ferrite Cement[J]. *Cement and Concrete Research*, 2017, 99: 8-17

[28] Gastaldi D, Paul G, Marchese L, *et al*. Hydration Products in Sulfoalu-Minate Cements: Evaluation of Amorphous Phases by XRD/Solid-state NMR[J]. *Cement and Concrete Research*, 2016, 90: 162-173

[29] Matschei T, Lothenbach B, Glasser FP. The AFm Phase in Portland Cement[J]. *Cement and Concrete Research*, 2007, 37: 118-130

[30] Murat M. Hydration Reaction and Hardening of Calcined Clays and Related Minerals. I. Preliminary Investigation on Metakaolinite[J]. *Cement and Concrete Research*, 1983, 13: 259-266

[31] Niu SW, Sun FN, Xie RZ, *et al*. Study on the Hydration Processes of High Belite Sulphoaluminate Cement using Electrochemical Impedance Spectroscopy[J]. *International Journal of Electrochemical Science*, 2020: 12 264-12 280

[32] Hu X, Shi CJ, Liu XJ, *et al*. A Review on Microstructural Characterization of Cement-based Materials by AC Impedance Spectroscopy[J]. *Cement and Concrete Composites*, 2019, 100: 1-14

[33] Niu SW, Han PJ, Sun FN, *et al*. Study of the Cement Hydration Processes in Coal Metakaolin and Cement Blends by Electrochemical Impedance Spectroscopy[J]. *International Journal of Electrochemical Science*, 2020: 9428-9445

[34] Madej D, Kruk A. Tracing the Early and Long-term Hydration of Fast Setting Cementitious Material (Ca7ZrAl6O18) and Calcium Aluminate Cement (CAC) Pastes by Means of Electrochemical Impedance Spectroscopy and Other Methods[J]. *Construction and Building Materials*, 2018, 164: 94-102

[35] Ford SJ, Hwang JH, Shane JD, *et al*. Dielectric Amplification in Cement Pastes[J]. *Advanced Cement Based Materials*, 1997, 5: 41-48

[36] Gu P, Xie P, Fu Y, *et al*. AC Impedance Phenomena in Hydrating Cement Systems: Frequency Dispersion Angle and Pore Size Distribution[J]. *Cement and Concrete Research*, 1994, 24: 86-88

[37] Xie P, Gu P, Xu ZZ, *et al*. A Rationalized AC Impedence Model for Microstructural Characterization of Hydrating Cement Systems[J]. *Cement and Concrete Research*, 1993, 23: 359-367

[38] Gu P, Xie P, Beaudoin JJ, *et al*. AC Impedance Spectroscopy (I): A New Equivalent Circuit Model for Hydrated Portland Cement Paste[J]. *Cement and Concrete Research*, 1992, 22: 833-840

[39] Husain A, Kupwade-Patil K, Al-Aibani AF, *et al*. In situ Electrochemical Impedance Characterization of Cement Paste with Volcanic Ash to Examine Early Stage of Hydration[J]. *Construction and Building Materials*, 2017, 133: 107-117

[40] Zhang YJ, Wang S, Li LP, *et al*. A Preliminary Study of the Properties of Potassium Phosphate Magnesium Cement-based Grouts Admixed with Metakaolin, Sodium Silicate and Bentonite[J]. *Construction and Building Materials*, 2020, 262: 119893